

Alma Mater Studiorum Università di Bologna  
Archivio istituzionale della ricerca

Exploitation of the Power Capability in a Five-Phase Doubly-Fed Induction Motor Drive for Contact-Less Energy Transfer

This is the final peer-reviewed author's accepted manuscript (postprint) of the following publication:

*Published Version:*

Rizzoli G., Mengoni M., Sala G., Vancini L., Zarri L., Tani A., et al. (2022). Exploitation of the Power Capability in a Five-Phase Doubly-Fed Induction Motor Drive for Contact-Less Energy Transfer. IEEE TRANSACTIONS ON INDUSTRIAL ELECTRONICS, 69(8), 7596-7606 [10.1109/TIE.2021.3109507].

*Availability:*

This version is available at: <https://hdl.handle.net/11585/833100> since: 2024-02-27

*Published:*

DOI: <http://doi.org/10.1109/TIE.2021.3109507>

*Terms of use:*

Some rights reserved. The terms and conditions for the reuse of this version of the manuscript are specified in the publishing policy. For all terms of use and more information see the publisher's website.

This item was downloaded from IRIS Università di Bologna (<https://cris.unibo.it/>).  
When citing, please refer to the published version.

(Article begins on next page)

This is the final peer-reviewed accepted manuscript of:

**G. Rizzoli *et al.*, "Exploitation of the Power Capability in a Five-Phase Doubly Fed Induction Motor Drive for Contact-Less Energy Transfer," in *IEEE Transactions on Industrial Electronics*, vol. 69, no. 8, pp. 7596-7606, Aug. 2022**

The final published version is available online at:

<https://doi.org/10.1109/TIE.2021.3109507>

Terms of use:

Some rights reserved. The terms and conditions for the reuse of this version of the manuscript are specified in the publishing policy. For all terms of use and more information see the publisher's website.

*This item was downloaded from IRIS Università di Bologna (<https://cris.unibo.it/>)*

***When citing, please refer to the published version.***

# Exploitation of the Power Capability in a Five-Phase Doubly-Fed Induction Motor Drive for Contact-Less Energy Transfer

G. Rizzoli, M. Mengoni, *Member, IEEE*, G. Sala, *Member, IEEE*, L. Vancini, L. Zarri, *Senior Member, IEEE*, A. Tani, R. Bojoi, *Fellow, IEEE*

**Abstract** - Rotary assembly stations are commonly used in automated manufacturing processes. These production platforms require the speed control of the plate and need power for the actuators and sensors located on the rotating frame. These requirements are usually met through a gearmotor and sliding electrical contacts. Among the solutions that avoid the slip-rings, this paper focuses on an integrated electric drive consisting of a gearless five-phase wound-rotor induction machine fed by two inverters, one placed on the stator reference frame and one placed on the rotating one. The main contribution is a novel control scheme that maximizes the power transferred to the rotating loads in compliance with the thermal constraint of the rotor and the voltage constraint of the rotor inverter. The theoretical analysis allows deriving an analytical solution to the control problem, and the experimental results confirm the effectiveness of the proposed algorithm.

**Index Terms** - Variable speed drives, induction motors, inductive power transmission.

## I. INTRODUCTION

Rotary assembly tables are machines used for the production of goods in industrial automation processes, such as bottle filling and capping systems. The core of an industrial rotary assembly station is a rotating disk, driven by a gearmotor, on which objects that must undergo sequential machining are positioned. When actuators and control sensors are positioned on the rotating plate, a system that supplies the electric loads located on the rotary table is required. Sliding electrical contacts are commonly used. However, sliding contacts are subject to wear [1] and require frequent maintenance and preventive replacement to ensure high reliability of the production line. Consequently, rotating transformers [2] and capacitive coupled systems [3]-[4] have been proposed as valid alternatives to slip-rings, allowing the contactless transmission of the power to the rotating loads.

A device that integrates both the power transmission and the propulsion functions is the direct-drive doubly-fed electrical machine. This concept is present in the literature for three-phase [5] and multiphase machines [6]-[7]. Compared to three-phase solutions, the use of multiphase machines guarantees lower torque ripple since multiple spatial harmonics of the magnetic field in the air gap can be controlled independently [8]. The angular speed and magnitude of these field harmonics can be varied by acting

appropriately on the phase currents [9]. Usually, the fundamental harmonic of the field generates the main driving torque, while higher-order harmonics provide additional features to the drive. Several papers regarding fault-tolerant [10]-[13], high torque-density [14], and sensorless drives [8], [15]-[16] are reported in the literature. Also, online diagnostic systems have been developed to assess the health status of multiphase motors [17]. The literature reports almost no references regarding the exploitation of the degrees of freedom of a multiphase induction machine to supply special loads through the rotor.

Extending the proof-of-concept proposed in [6]-[7] for the control of a rotary assembly platform by using a doubly-fed five-phase induction machine, this paper proposes an optimized control system suitable for industrial applications. Such a system uses the fundamental spatial component of the field in the airgap to control the torque and speed of the rotor, while the third harmonic is used to transfer energy to the rotating loads. The integrated drive developed in this paper can be regarded as a two-port energy hub. The use of multi-port multiphase machines as energy hubs has already been proposed [18] but, in those solutions, all the systems involved in the power exchange were connected to the stator windings.

Compared with [6]-[7], the contributions of the present paper are:

- the current and voltage constraints related to the rotor winding and the rotor inverter are considered and implemented in the control system;
  - the optimal drive performance is analyzed through a graphical approach;
  - development of a novel rotor control strategy for power transfer to rotating loads, minimizing the rotor Joule losses.
- The proposed control system allows one to increase the power delivered to the rotor loads by 200% under the same operating constraints.

The rest of this paper is organized as follows. In Section II, the mathematical model of the electrical machine and the related control law are derived. In Section III, the new proposed control algorithm is described. Before outlining the conclusion of the work, Section IV illustrates the experimental results obtained with a laboratory prototype.

## II. DESCRIPTION OF THE SYSTEM

The electric drive proposed for rotary assembly platforms is shown in Fig. 1. The system is composed of a gearless five-phase wound-rotor induction machine connected to two five-phase inverters, one placed on the stationary frame and one placed on the rotating one. The stator inverter is fed by the mains through an ac/dc converter, while the rotor inverter extracts power from the machine and supplies the loads and actuators placed on the rotating disk.

Manuscript received March 8, 2021; revised June 3, 2021 and July 26, 2021; accepted August 13, 2021.

G. Rizzoli, M. Mengoni, G. Sala, L. Vancini, L. Zarri, A. Tani are with the Department of Electrical, Electronic and Information Engineering "G. Marconi", University of Bologna, Bologna, 40136, Italy (e-mail: [gabriele.rizzoli@unibo.it](mailto:gabriele.rizzoli@unibo.it), [michele.mengoni@unibo.it](mailto:michele.mengoni@unibo.it), [g.sala@unibo.it](mailto:g.sala@unibo.it), [luca.vancini4@unibo.it](mailto:luca.vancini4@unibo.it), [luca.zarri2@unibo.it](mailto:luca.zarri2@unibo.it), [angelo.tani@unibo.it](mailto:angelo.tani@unibo.it)).

R. Bojoi is with the Department of Energy "G. Ferraris", Politecnico di Torino, 10129, Turin, Italy ([radu.bojoi@polito.it](mailto:radu.bojoi@polito.it)).

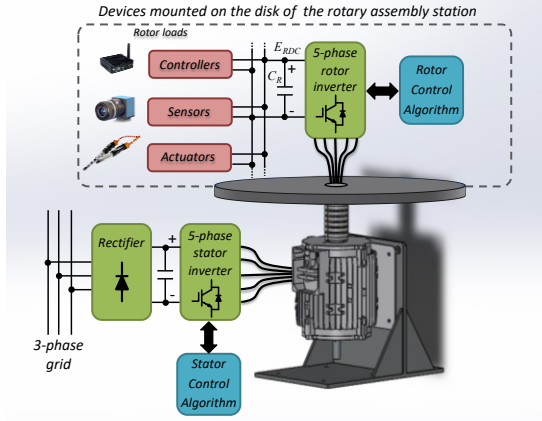


Fig. 1- Scheme of the five-phase wound-rotor induction motor drive.

### A. Five-Phase Induction Machine Model

A generic five-phase induction machine with distributed windings and star-connected phases can be analyzed through the Vector Space Decomposition (VSD) [9]. The following set of complex equations describes the machine in the fundamental and the third harmonic subspaces:

$$\bar{v}_{S1} = R_S \bar{i}_{S1} + j\omega_1 \bar{\varphi}_{S1} + \frac{d\bar{\varphi}_{S1}}{dt} \quad (1)$$

$$\bar{v}_{R1} = R_R \bar{i}_{R1} + j(\omega_1 - \omega_m) \bar{\varphi}_{R1} + \frac{d\bar{\varphi}_{R1}}{dt} \quad (2)$$

$$\bar{\varphi}_{S1} = L_{S1} \bar{i}_{S1} + M_1 \bar{i}_{R1} \quad (3)$$

$$\bar{\varphi}_{R1} = M_1 \bar{i}_{S1} + L_{R1} \bar{i}_{R1} \quad (4)$$

$$\bar{v}_{S3} = R_S \bar{i}_{S3} + j\omega_3 \bar{\varphi}_{S3} + \frac{d\bar{\varphi}_{S3}}{dt} \quad (5)$$

$$\bar{v}_{R3} = R_R \bar{i}_{R3} + j(\omega_3 - 3\omega_m) \bar{\varphi}_{R3} + \frac{d\bar{\varphi}_{R3}}{dt} \quad (6)$$

$$\bar{\varphi}_{S3} = L_{S3} \bar{i}_{S3} + M_3 \bar{i}_{R3} \quad (7)$$

$$\bar{\varphi}_{R3} = M_3 \bar{i}_{S3} + L_{R3} \bar{i}_{R3} \quad (8)$$

where  $\bar{v}_{Sk}$  and  $\bar{v}_{Rk}$  ( $k=1,3$ ) are the multiple space vectors of the stator and rotor voltages,  $\bar{i}_{Sk}$  and  $\bar{i}_{Rk}$  ( $k=1,3$ ) are the multiple space vectors of the stator and rotor currents,  $\bar{\varphi}_{Sk}$  and  $\bar{\varphi}_{Rk}$  ( $k=1,3$ ) are the multiple space vectors of the stator and rotor fluxes,  $\omega_m$  is the electric angular speed of the rotor,  $R_S$  and  $R_R$  are the stator and rotor phase resistances, and  $L_{Sk}$ ,  $L_{Rk}$  and  $M_k$  ( $k=1,3$ ) are the self and mutual inductances of the stator and rotor windings. Equations (1)-(4) and (5)-(8) are written respectively in the generic reference frames  $d_1-q_1$  and  $d_3-q_3$  with electrical angular speeds  $\omega_1$  and  $\omega_3$ , which are chosen as explained in Sections II.B and II.C.

The sets of equations (1)-(4) and (5)-(8) are independent of one another. Therefore, from the mathematical point of view, the five-phase induction machine is equivalent to two three-phase machines, with different electric parameters and pole pairs, which generate a magnetic field in the same air gap and exert their torque on the same mechanical shaft. The total torque can be written as the sum of two terms:

$$T = T_1 + T_3 \quad (9)$$

where

$$T_1 = \frac{5}{2} p (j\bar{\varphi}_{S1} \cdot \bar{i}_{S1}) \quad (10)$$

$$T_3 = \frac{5}{2} p (3j\bar{\varphi}_{S3} \cdot \bar{i}_{S3}) \quad (11)$$

The symbol  $p$  is the number of pairs of poles, the dot operator " $\cdot$ " is the product of the magnitude of two vectors, and the cosine of the angle between them.

The equation of the motion can be written as follows:

$$\frac{d\omega_m}{dt} = p \frac{T_1 + T_3 - T_B}{J} \quad (12)$$

where  $J$  is the total moment of inertia of the system, and  $T_B$  is the total braking torque of the mechanical load.

The fundamental spatial harmonic of the magnetic field, which is related to (1)-(4), is used to control the motion of the rotor, whereas the third spatial harmonic of the field, which is related to (5)-(8), is used to transfer electric power to the rotating loads.

### B. Torque Control

If  $T_3$  is negligible, the motion can be controlled by acting only on  $T_1$ . If the rotor inverter applies a voltage  $\bar{v}_{R1}$  equal to zero, (1)-(4) describe an equivalent three-phase induction machine with short-circuited rotor winding. Therefore, the primary torque contribution  $T_1$  can be controlled by using a traditional rotor field-oriented control scheme. This solution is convenient because it does not require a continuous exchange of information between the stator and the rotor control systems.

The torque  $T_1$  is controlled in rotating reference frame  $d_1-q_1$  whose d-axis is aligned with the flux  $\bar{\varphi}_{R1}$ .

With  $\bar{v}_{R1}$  equal to zero, the following scalar expression of the rotor flux magnitude can be obtained by combining (2) and (4):

$$\tau_{R1} \frac{d\varphi_{R1}}{dt} + \varphi_{R1} = M_1 i_{S1d} \quad (13)$$

where  $i_{S1d}$  is the d-component of the stator current vector  $\bar{i}_{S1}$ , and  $\tau_{R1}$  is the rotor time constant  $L_{R1}/R_R$ .

By combining (3), (4), and (13) into (10), the torque  $T_1$  can be written as:

$$T_1 = \frac{5}{2} p \frac{M_1}{L_{R1}} \varphi_{R1} i_{S1q} \quad (14)$$

Therefore, the torque  $T_1$  and rotor flux  $\varphi_{R1d}$  can be controlled by the components of the stator current vector  $\bar{i}_{S1}$ .

### C. Generation of a DC-Voltage for the Rotor Loads

As shown in Fig. 1, the electric loads and actuators placed on the rotating disk of the assembly station can be powered by the rotor inverter dc-link, whose electrostatic energy must be kept constant. The power balance on the capacitor  $C_R$  can be written as:

$$\frac{d}{dt} \left( \frac{1}{2} C_R E_{RDC}^2 \right) = P_R - P_{LOAD} \quad (15)$$

where  $E_{RDC}$  is the voltage across  $C_R$ ,  $P_{LOAD}$  is the total power absorbed by the auxiliary rotor loads, and  $P_R$  is the power extracted from the rotor winding of the machine by the rotor inverter. By controlling  $P_R$ , it is possible to provide a stable voltage source for the auxiliary loads.

Under the assumption that  $\bar{v}_{R1}$  is equal to zero, the active and reactive powers  $P_R$  and  $Q_R$  extracted from the rotor winding by the inverter depend only on the third spatial harmonic of the magnetic field:

$$P_R = -\frac{5}{2} \bar{v}_{R3} \cdot \bar{i}_{R3} \quad (16)$$

$$Q_R = -\frac{5}{2} \bar{v}_{R3} \cdot j\bar{i}_{R3} \quad (17)$$

It is worth noting that  $P_R$  is transferred to the rotor from the stator winding across the air-gap. Therefore, the control system of the stator inverter must be coordinated with that of the rotor inverter. A suitable method for controlling  $P_R$  is to inject a rotating space vector  $\bar{i}_{S3}^S$  into the stator winding:

$$\bar{i}_{S3}^S = I_{S3} e^{j\omega_3 t}. \quad (18)$$

The vectors with superscript ‘‘S’’ and ‘‘R’’ represent quantities respectively in the stator and rotor  $\alpha$ - $\beta$  reference frames, while the vector quantities without any superscript are defined in rotating reference frames whose positions are identified by  $\theta_1$  and  $\theta_3$ .

The current magnitude  $I_{S3}$  in (18) is assumed constant, and the angular frequency  $\omega_3$  is equal to:

$$\omega_3 = 3\omega_m + \Delta\omega_3. \quad (19)$$

The parameter  $\Delta\omega_3$  represents the slip between the angular speed of the magnetic field generated by the stator current  $\bar{i}_{S3}^S$  and the mechanical speed of the motor. Therefore, if  $\Delta\omega_3$  is constant, the current  $\bar{i}_{S3}^R$  written in a reference frame synchronous to the rotor becomes

$$\bar{i}_{S3}^R = \bar{i}_{S3}^S e^{-j3\omega_m t} = I_{S3} e^{j\Delta\omega_3 t}, \quad (20)$$

which represents a rotating current space vector with constant magnitude  $I_{S3}$  and angular speed  $\Delta\omega_3$  independent of the mechanical speed of the motor shaft. By substituting (8) in (6), the following rotor voltage equation can be derived:

$$\begin{aligned} \bar{v}_{R3} = & R_{R3} \bar{i}_{R3} + L_{R3} \frac{d\bar{i}_{R3}}{dt} + M_3 \frac{d\bar{i}_{S3}}{dt} + \\ & + j(\omega_3 - 3\omega_m) L_{R3} \bar{i}_{R3} + j(\omega_3 - 3\omega_m) M_3 \bar{i}_{S3}. \end{aligned} \quad (21)$$

If  $\Delta\omega_3$  and  $I_{S3}$  are constant, in a reference frame  $d_3$ - $q_3$  whose d-axis has the same direction of  $j\bar{i}_{S3}^S$ , (21) can be simplified as follows:

$$\bar{v}_{R3} = R_{R3} \bar{i}_{R3} + L_{R3} \frac{d\bar{i}_{R3}}{dt} + j\Delta\omega_3 L_{R3} \bar{i}_{R3} + v_{exc} \quad (22)$$

where the excitation voltage  $v_{exc}$  is the following real constant:

$$v_{exc} = \Delta\omega_3 M_3 I_{S3}. \quad (23)$$

It can be noted that (22) is similar to the Kirchhoff equation of a grid-connected three-phase synchronous rectifier, where voltage  $v_{exc}$  substitutes the grid voltage, and the machine parameters  $R_{R3}$  and  $L_{R3}$  can be considered as the parameters of an equivalent inductive line filter. Voltage  $v_{exc}$  is constant if the current vector  $\bar{i}_{S3}^S$  injected into the stator winding rotates on a circle of radius  $I_{S3}$  and at variable angular speed  $3\omega_m + \Delta\omega$ , as stated in (18).

By replacing (22) in (16)-(17) under the assumption of steady state conditions, one finds:

$$P_R = -\frac{5}{2} \left( R_{R3} |\bar{i}_{R3}|^2 + v_{exc} i_{R3d} \right) \quad (24)$$

$$Q_R = -\frac{5}{2} \left( \Delta\omega_3 L_{R3} |\bar{i}_{R3}|^2 - v_{exc} i_{R3q} \right). \quad (25)$$

Equation (24) and (25) show that the active power  $P_R$  delivered to the rotor inverter can be controlled by the d-component of the rotor current  $\bar{i}_{R3}$ , while the reactive power  $Q_R$  can be adjusted through  $i_{R3q}$ . Therefore,  $P_R$  and  $Q_R$  can be controlled by the rotor current  $\bar{i}_{R3}$ . As a side effect, the

control of the active and reactive power generates a torque disturbance  $T_3$ , which is produced by the interaction between  $\bar{i}_{S3}$  and  $\bar{i}_{R3}$ . By replacing (7) in (11) and considering (23), it can be verified that the instantaneous value of  $T_3$  is

$$T_3 = -\frac{15}{2} p \frac{v_{exc} i_{R3d}}{\Delta\omega_3}. \quad (26)$$

Equation (26) can be combined with (24), as follows:

$$T_3 = 5 p \frac{P_{T3}}{\Delta\omega_3}, \quad (27)$$

where  $P_{T3}$  is the total power transferred from the stator winding to the rotor winding, equal to the sum of the rotor copper loss  $P_{JR3}$  and the power  $P_R$ , as follows:

$$P_{T3} = \frac{5}{2} R_{R3} |\bar{i}_{R3}|^2 + P_R = P_{JR3} + P_R. \quad (28)$$

If the copper loss  $P_{JR3}$  is negligible, the torque disturbance  $T_3$  is proportional to  $P_R$  and reduces if the angular frequency  $\Delta\omega_3$  increases. Therefore, for the same level of  $P_R$ , the higher  $\Delta\omega_3$ , the lower the magnitude of  $T_3$ . It is worth noting that  $T_3$  is constant at steady state. Therefore, it can be treated as a torque disturbance and its effect can be compensated for by the speed control loop implemented in the fundamental subspace.

In conclusion, while the rotor inverter behaves as an active power rectifier in subspace  $d_3$ - $q_3$  and keeps the rotor dc-link voltage constant, the stator inverter implements a standard rotor field-oriented control in subspace  $d_1$ - $q_1$  and generates a current vector  $\bar{i}_{S3}$  that rotates at speed  $3\omega_m + \Delta\omega_3$  for a stationary observer.

#### D. Active and Reactive Power Control Strategy

As shown in Section II.B, no assumption about the reactive power are made. Therefore,  $Q_R$  can be used to maximize the performance of the electric drive. A useful approach to understand the effect of the reactive power control on the operation of the machine is to draw the loci of constant power  $P_R$  and  $Q_R$  in a complex plane, where the horizontal and vertical axes are the control variables  $i_{R3d}$  and  $i_{R3q}$ . The equation of the rotor reactive power (25) can be rearranged as follows:

$$i_{R3d}^2 + \left( i_{R3q} - \frac{v_{exc}}{2\Delta\omega_3 L_{R3}} \right)^2 = \left( \frac{v_{exc}}{2\Delta\omega_3 L_{R3}} \right)^2 - \frac{2}{5} \frac{Q_R}{\Delta\omega_3 L_{R3}}. \quad (29)$$

Equation (29) represents a circle. The coordinates of its center  $(x_{Q_R}, y_{Q_R})$  and the dimension of its radius  $r_{Q_R}$  in the

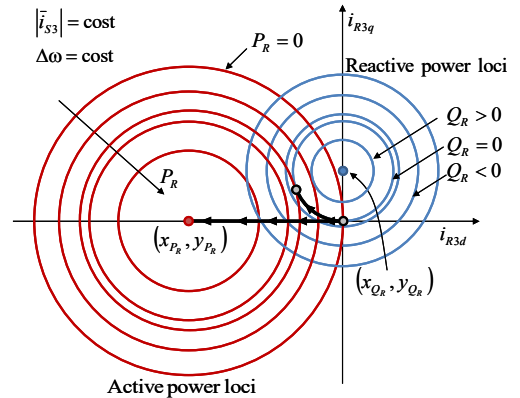


Fig. 2. Loci of points with constant active power  $P_R$  and constant reactive power  $Q_R$  in the  $i_{R3d}$  -  $i_{R3q}$  plane.



$i_{R3d} - i_{R3q}$  plane are as follows:

$$\begin{cases} x_{Q_R} = 0, y_{Q_R} = \frac{v_{exc}}{2\Delta\omega_3 L_{R3}} \\ r_{Q_R}^2 = \left( \frac{v_{exc}}{2\Delta\omega_3 L_{R3}} \right)^2 - \frac{2}{5} \frac{Q_R}{\Delta\omega_3 L_{R3}} \end{cases} \quad (30)$$

It is worth noting that the center does not depend on the angular speed  $\Delta\omega_3$  owing to (23). Therefore, if the magnitude of the stator current  $\bar{i}_{s3}$  is constant, the center of the circle is fixed, and the radius  $r_{Q_R}$  increases as long as the reactive power  $Q_R$  decreases, as depicted in Fig. 2. The upper bound for the reactive power can be obtained from the following intrinsic constraint:

$$r_{Q_R}^2 = \left( \frac{v_{exc}}{2\Delta\omega_3 L_{R3}} \right)^2 - \frac{2}{5} \frac{Q_R}{\Delta\omega_3 L_{R3}} \geq 0 \quad (31)$$

which leads to:

$$Q_R \leq \frac{5}{8} \frac{v_{exc}^2}{\Delta\omega_3 L_{R3}}. \quad (32)$$

The upper bound (32) corresponds to the condition in which the circle collapses into point  $(x_{Q_R}, y_{Q_R})$ .

Similarly, the loci of constant power  $P_R$  in the complex plane  $i_{R3d} - i_{R3q}$  are represented by the red circles shown in Fig. 2. In fact, (24) can be rewritten as follows:

$$\left( i_{R3d} + \frac{v_{exc}}{2R_R} \right)^2 + i_{R3q}^2 = \left( \frac{v_{exc}}{2R_R} \right)^2 - \frac{2}{5} \frac{P_R}{R_R} \quad (33)$$

where the coordinates of the center  $(x_{P_R}, y_{P_R})$  and the radius  $r_{P_R}$  are

$$\begin{cases} x_{P_R} = -\frac{v_{exc}}{2R_R}, y_{P_R} = 0 \\ r_{P_R}^2 = \left( \frac{v_{exc}}{2R_R} \right)^2 - \frac{2}{5} \frac{P_R}{R_R} \end{cases} \quad (34)$$

It can be observed that the radius of the circle decreases if  $P_R$  increases. The upper bound for the rotor active power can be obtained by noting that  $r_{P_R}^2$  in (34) is positive:

$$P_R \leq \frac{5}{8} \frac{v_{exc}^2}{R_R}. \quad (35)$$

The upper bound (35) represents the theoretical maximum active power that can be transferred to the rotor loads and corresponds to the condition in which the circle collapses into point  $(x_{P_R}, y_{P_R})$ .

The admissible operating points of the drive are the intersections between the circles of constant active and reactive power. It is worth noting that the reference value of  $P_R$ , which is equal to  $P_{LOAD}$  at steady state, can be obtained with different values of the reactive power. A solution, which was used in [6], is to set  $Q_R$  equal to zero to minimize the power rating of the rotor inverter. This choice implies that the possible operating points of the electric drive lay on the blue circle with a zero value of  $Q_R$  depicted in Fig. 2. Under this condition, the upper bound (35) for the active power cannot be reached because the maximum power obtainable from the rotor winding corresponds to the tangency condition between the circles at constant power  $P_R$  and null reactive power ( $Q_R = 0$ ).

In this paper, a different method to control  $Q_R$  is

presented. Clearly,  $Q_R$  affects the maximum power that can be extracted from the rotor winding and the Joule loss  $P_{JR3}$  of the rotor:

$$P_{JR3} = \frac{5}{2} R_R (i_{R3d}^2 + i_{R3q}^2). \quad (36)$$

For a given level of  $P_R$ , the loss  $P_{JR3}$  is minimized when the distance between  $\bar{i}_{R3}$  and the origin of the complex plane  $i_{R3d} - i_{R3q}$  is the shortest. This condition is obtained when the current component  $i_{R3q}$  is equal to zero. By imposing  $i_{R3q} = 0$  in (25), one finds:

$$Q_R = -\frac{5}{2} \Delta\omega_3 L_{R3} i_{R3d}^2. \quad (37)$$

Equation (37) states that the losses  $P_{JR3}$  are minimized when the rotor inverter compensates the reactive power of the inductance  $L_{R3}$ . When (37) is imposed, the maximum (35) for  $P_R$  can be theoretically reached. Therefore, the ideal trajectory of  $\bar{i}_{R3}$  in the complex plane  $i_{R3d} - i_{R3q}$  is a segment that starts from the origin when  $P_R$  is zero and reaches  $-v_{exc}/2R_R$  when  $P_R$  equals its maximum defined in (35). A graphical example of the ideal trajectory of  $\bar{i}_{R3}$  is shown in Fig. 2. However, the admissible operating points must also satisfy the thermal constraint of the rotor current

$$i_{R3d}^2 + i_{R3q}^2 \leq I_{R3max}^2 \quad (38)$$

and the voltage constraint of the rotor inverter

$$v_{R3d}^2 + v_{R3q}^2 \leq V_{R3max}^2. \quad (39)$$

Current  $I_{R3max}$  represents the thermal current limit of the rotor winding while  $V_{R3max}$  is the maximum voltage that can be synthesized by a multiphase inverter in the linear modulating region, as discussed in [19]. For a five-phase inverter, if  $\bar{v}_{R1}$  is equal to zero, the maximum amplitude of the rotor phase voltages  $V_{R3max}$  is:

$$V_{R3max} = \frac{E_{RDC}}{2 \sin\left(\frac{2}{5} \pi\right)}. \quad (40)$$

By substituting the voltage components  $v_{R3d}$  and  $v_{R3q}$  of (22) in (39) and considering the system at steady state, the following inequality can be obtained:

$$\left( i_{R3d} + \frac{R_R v_{exc}}{R_R^2 + \Delta\omega_3^2 L_{R3}^2} \right)^2 + \left( i_{R3q} - \frac{\Delta\omega_3 L_{R3} v_{exc}}{R_R^2 + \Delta\omega_3^2 L_{R3}^2} \right)^2 \leq \frac{V_{R3max}^2}{R_R^2 + \Delta\omega_3^2 L_{R3}^2} \quad (41)$$

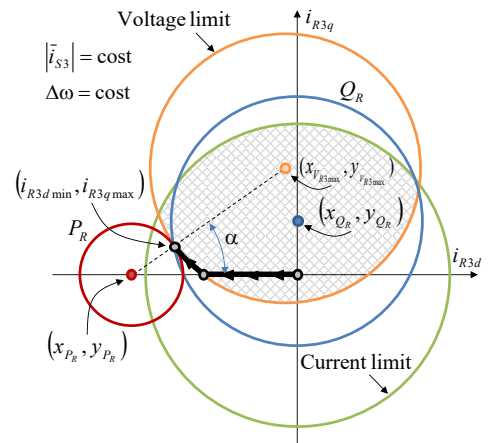


Fig. 3. Trajectory followed by current  $\bar{i}_{R3}$  considering the current and voltage constraints of the rotor windings and the rotor inverter.

which represents the implicit equation of the voltage limit depicted in Fig. 3. The coordinates of the center  $(x_{V_{R3\max}}, y_{V_{R3\max}})$  and the radius  $r_{V_{R3\max}}$  of the circle are:

$$\begin{cases} x_{V_{R3\max}} = -\frac{R_R v_{exc}}{R_R^2 + \Delta\omega_3^2 L_{R3}^2}, y_{V_{R3\max}} = \frac{\Delta\omega_3 L_{R3} v_{exc}}{R_R^2 + \Delta\omega_3^2 L_{R3}^2} \\ r_{V_{R3\max}}^2 = \frac{V_{R3\max}^2}{R_R^2 + \Delta\omega_3^2 L_{R3}^2} \end{cases} \quad (42)$$

The admissible operating states of the machine, represented by the shaded region of Fig. 3, must lay inside the area of intersection between the current limit circle and the voltage limit circle, defined respectively by (38) and (41). The trajectory that minimizes the Joule losses of the rotor can be traveled up to the upper bound (35) only if the circles that represent the voltage and current limits embrace the center of the circle that represents the locus of states with constant  $P_R$ .

If the current limit (38) is stricter than the voltage limit (39), the maximum power that can be transferred to the rotor loads can be found by imposing  $i_{R3d} = -I_{R3\max}$  in (24) as follows:

$$P_{R\max} = -\frac{5}{2} \left( R_R I_{R3\max}^2 - v_{exc} I_{R3\max} \right). \quad (43)$$

Conversely, when the voltage limit is more stringent than the current limit,  $P_R$  can increase further only if  $\bar{i}_{R3}$  follows a trajectory that belongs to the circumference of the voltage limit depicted in Fig. 3. Two further operating limits may be encountered on this trajectory. The former is the thermal constraint of the rotor current (38); the latter is the constraint on the rotor active power (35). As  $P_R$  increases the limit that is first encountered depends on the actual parameters of the drive.

In the first case, the maximum power occurs when the rotor inverter entirely exploits the dc-bus voltage  $E_{DCR}$ ,  $\bar{i}_{R3}$  is on the voltage circle and its magnitude is  $I_{R3\max}$ .

In the second case, the maximum value for  $P_R$  is encountered before reaching the rotor rated thermal current. This condition may happen if the circle that represents the loci of points at constant active power becomes tangent to the circle of the voltage limit. This operating condition is shown in Fig. 3, and the components of  $\bar{i}_{R3}$  can be geometrically deduced as follows:

$$\tan \alpha = \frac{y_{V_{R3\max}}}{x_{P_R} - x_{V_{R3\max}}} = \frac{2R_R \Delta\omega_3 L_{R3}}{\Delta\omega_3^2 L_{R3}^2 - R_R^2} \quad (44)$$

$$i_{R3d\min} = -\frac{R_R v_{exc}}{R_R^2 + \Delta\omega_3^2 L_{R3}^2} - \frac{V_{R3\max} \cos \alpha}{\sqrt{R_R^2 + \Delta\omega_3^2 L_{R3}^2}} \quad (45)$$

$$i_{R3q\max} = \frac{\Delta\omega_3 L_{R3} v_{exc}}{R_R^2 + \Delta\omega_3^2 L_{R3}^2} - \frac{V_{R3\max} \sin \alpha}{\sqrt{R_R^2 + \Delta\omega_3^2 L_{R3}^2}}. \quad (46)$$

The maximum power can be calculated by substituting the components (45) and (46) of the current  $\bar{i}_{R3}$  in (24). Any attempt to follow the trajectory of the voltage limit beyond point  $(i_{R3d\min}, i_{R3q\max})$  involves a reduction in the power  $P_R$ . This characteristic may lead to the instability of the control system due to the non-monotonous behavior of  $P_R$ . Also, point  $(i_{R3d\min}, i_{R3q\max})$  can be reached only if the thermal constraint for the rotor currents (38) is satisfied.

### III. CONTROL SYSTEM

The control system of the proposed electric drive is shown in Fig. 4. It consists of two independent parts that are implemented in two different control boards for the stator and rotor inverters. It results that the two controllers are not synchronized and do not share any information about their state variables.

#### A. Speed and Torque Control

The speed and torque are regulated by a cascade control implemented on the stator inverter. The block diagram of Fig. 4 illustrates the external speed controller (a) and the two internal current regulators (b)-(c) for the torque and flux control. In cascaded control, the bandwidth of the outer loop should be lower than the bandwidth of the inner loop. The primary torque contribution  $T_1$  is controlled by a traditional direct vector control scheme implemented in a reference frame with the d-axis aligned with the rotor flux  $\bar{\phi}_{R1}$ , as described in Section II.B. The error between the reference speed  $\omega_{m,ref}$  and the actual one is sent to the PI controller (a), which generates the setpoint  $i_{S1d,ref}$ . In order to guarantee high torque dynamics, the magnitude of the rotor flux  $\phi_{R1}$  in (14) is kept constant by setting the current reference  $i_{S1d,ref}$  to its rated value. The current references  $i_{S1d,ref}$  and  $i_{S1q,ref}$  are tracked by the PI controllers (b) and (c). Moreover, the estimated back-electromotive forces  $v_{S1d,comp}$  and  $v_{S1q,comp}$  of the machine are added up to the output signals of the PI current controllers to create the reference voltages  $v_{S1d,ref}$  and  $v_{S1q,ref}$ . The feed-forward compensation of the back-EMF has been implemented to improve the bandwidth of the current control loops.

The implementation of the vector control scheme requires the knowledge of the magnitude and the position of the rotor flux  $\bar{\phi}_{R1}^S$ . The magnitude  $\phi_{R1}$ , angular position  $\theta_1$ , and angular speed  $\omega_1$  of  $\bar{\phi}_{R1}^S$  are estimated by means of a direct rotor flux observer based on (2) and (4) written in a reference frame synchronous with the rotor speed. The mechanical position of the rotor is sensed by an incremental encoder, while the mechanical speed is obtained as the derivative of the mechanical angle. Also, the equations of the flux observer assume that the rotor inverter keeps the voltage  $\bar{v}_{R1}$  equal to zero as if the rotor windings were short-circuited.

#### B. Control of the Rotor Power

The third spatial harmonic of the magnetic field in the airgap is used to transfer electric power from the stationary reference frame to the rotating one, as shown in Section II. The task of the stator inverter is to generate a current vector  $\bar{i}_{S3}^S$ , defined in (18), which rotates at angular speed  $\omega_3$ . For the tracking of the reference current, the PI regulators (e)-(f) have been implemented in an arbitrary reference frame  $d_3-q_3$  rotating at speed  $\omega_3$ , whose angular position can be calculated by integrating (19). The reference current  $i_{S3d,ref}$  is equal to the current magnitude  $I_{S3}$ , while the current component  $i_{S3q,ref}$  is set to zero. The feed forward compensation of the back electromotive force of the machine has been added to the output of the PI current controllers to improve the dynamic performance of the current control loop. The compensating terms  $v_{S3d,comp}$  and  $v_{S3q,comp}$  can be calculated as:

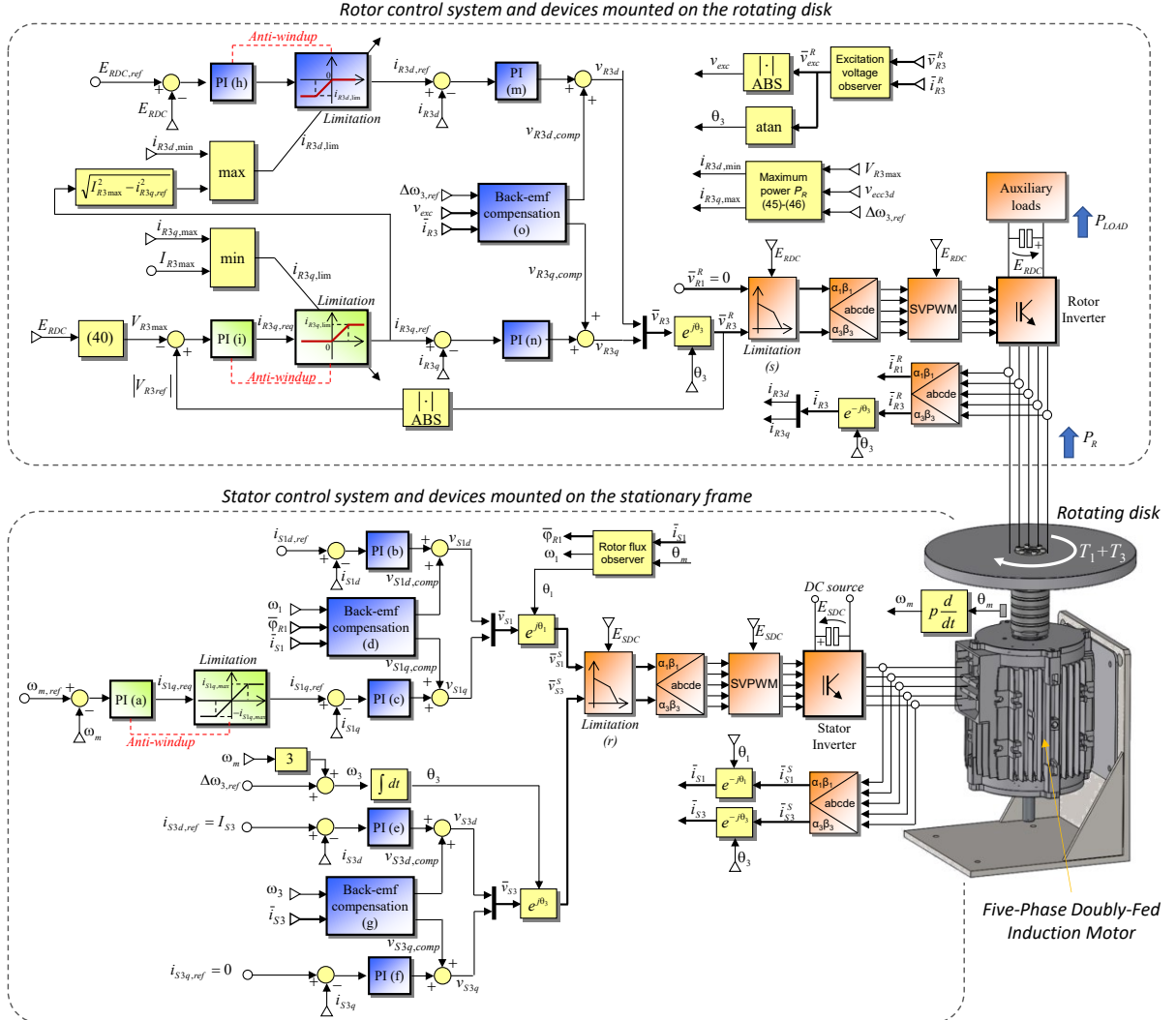


Fig. 4- Block diagram of the control system and schematics of the five-phase doubly-fed induction motor drive.

$$\begin{cases} v_{S3d,comp} = -\omega_3 L_{S3} i_{S3q} \\ v_{S3q,comp} = \omega_3 L_{S3} i_{S3d} \end{cases} \quad (47)$$

Once  $\bar{v}_{S1}$  and  $\bar{v}_{S3}$  are known, the modulating signals of the stator inverter can be synthesized through a pulse-width modulation technique. Furthermore, limitation block (r) ensures the operation of the inverter in the linear modulation region [19].

The control scheme of the rotor inverter is depicted in the upper part of Fig. 4. It can be observed that the reference voltage  $\bar{v}_{R1}$  is set to zero in order to emulate the short circuit of the rotor winding in the fundamental subspace, as discussed in Section II. Therefore, the main computational efforts of the rotor control system are devoted to the control of the power delivered to the rotor loads.

The proposed method for controlling  $P_R$  is based on the control of the d-q components of the rotor current  $\bar{i}_{R3}$  written in a reference frame with the d-axis aligned with the current vector  $j\bar{i}_{S3}^R$ . Since the rotor controller cannot receive the measurement of the stator current, an estimation of  $\bar{i}_{S3}^R$  can be found by integrating (6) and solving (8):

$$\bar{i}_{S3}^R = \frac{\bar{\varphi}_{R3}^R - L_{R3} \bar{i}_{R3}^R}{M_3} \quad (48)$$

The rotor flux  $\bar{\varphi}_{R3}^R$  can be obtained as follows:

$$\bar{\varphi}_{R3}^R = \frac{\bar{v}_{R3}^R - R_R \bar{i}_{R3}^R}{s} \quad (49)$$

where  $s$  is the Laplace variable. Therefore, the stator current seen from the rotor reference frame  $\bar{i}_{S3}^R$  can be estimated using only quantities measured on the rotating part of the drive. However, (49) cannot be used in actual system since errors and offsets in the acquired voltages and currents may accumulate at the integrator output, leading to the instability of the rotor flux observer [20].

In the proposed control scheme, the angular speed of the current  $\bar{i}_{S3}^R$  is constant and equal to  $\Delta\omega_3$ , according to (20). The electrical quantities in (49) are rotating vectors at angular speed  $\Delta\omega_3$ . Thus, the ideal integrator can be replaced by a low-pass filter that shows a finite gain at low frequency and behaves like an integrator at angular speed  $\Delta\omega_3$ :

$$\bar{\varphi}_{R3}^R = \frac{\tau_f}{1 + \tau_f s} (\bar{v}_{R3}^R - R_R \bar{i}_{R3}^R) \quad (50)$$

The time constant  $\tau_f$  of the filter must be selected so that

$$\frac{1}{\tau_f} < \frac{1}{10} \Delta\omega_3 \quad (51)$$

Once the estimated current  $\bar{i}_{S3}^R$  is available, the excitation voltage vector  $\bar{v}_{exc}^R$  can be calculated as:

$$\bar{v}_{exc}^R = jM_3 \Delta\omega_3 \bar{i}_{S3}^R \quad (52)$$



The real and imaginary components of vector  $\bar{v}_{exc}^R$  are used to find the angular position  $\theta_{R3}$  of the reference frame adopted for the control of the active and reactive powers  $P_R$  and  $Q_R$ , as described in Section II.

Two PI current controllers, (m) and (n), track the references  $i_{R3d,ref}$  and  $i_{R3q,ref}$  by generating the components  $v_{R3d}$  and  $v_{R3q}$  of the voltage vector  $\bar{v}_{R3}$ . The feed forward compensation of the back electromotive force of the machine have been added to the output of the PI controllers to improve the dynamic performance of the current control loop. The compensating terms  $v_{R3d,comp}$  and  $v_{R3q,comp}$  can be calculated as:

$$\begin{aligned} v_{R3d,comp} &= v_{exc} - \Delta\omega L_{R3} i_{R3q} \\ v_{R3q,comp} &= \Delta\omega L_{R3} i_{R3d} \end{aligned} \quad (53)$$

The current references  $i_{R3d,ref}$  and  $i_{R3q,ref}$  are generated by two control loops. The task of the first loop is the regulation of the voltage of the dc bus  $E_{RDC}$  by acting on  $i_{R3d,ref}$ . In fact, keeping  $E_{RDC}$  constant means that, at a steady state, the active power  $P_R$  is equal to the power absorbed by the rotor loads in (15). The task of the second regulation loop is to generate the current reference  $i_{R3q,ref}$ . If the magnitude of the reference voltage  $\bar{v}_{R3}$  is compatible with the voltage constraint (40), the current  $i_{R3q,ref}$  is kept at zero by the PI regulator (i) in order to minimize the rotor Joule loss. Otherwise, the PI regulator generates a positive current reference  $i_{R3q,ref}$  that allows respecting the constraint in (40).

The outputs of the PI regulators (h) and (i) are dynamically bounded to satisfy the most stringent limit between the rotor current constraint (38) and the stability constraint related to the maximum power that can be transferred to the rotor loads. The current components  $i_{R3d,min}$  and  $i_{R3q,max}$  that maximize the power  $P_R$ , subjected to the voltage constraint (41), can be calculated through (45) - (46).

It is worth noting that the stator and rotor inverters actively control the currents  $\bar{i}_{s3}$  and  $\bar{i}_{r3}$ . The control method proposed in this paper assumes that the excitation voltage  $v_{exc}$  is constant regardless of the perturbations introduced by the rotor control system. Therefore, the stator current controllers (e) and (f) must be very effective in keeping the current  $\bar{i}_{s3}$  equal to its reference (18). For this reason, the control bandwidth of  $\bar{i}_{s3}$  must be wider than that of the rotor current  $\bar{i}_{r3}$ .

The control diagram illustrated in Fig. 4 has been utilized as a roadmap for the implementation of the control algorithm used to carry out the experimental tests presented in the next section.

#### IV. EXPERIMENTAL RESULTS

Fig. 5 shows the demonstrator of the electric drive for rotary assembly platforms used to test the proposed control algorithm. The drive consists of a five-phase doubly-fed induction motor, two five-phase inverters, a rotating disk, and an active dc load. The parameters of the electric machine have been experimentally evaluated and are reported in Table I while the parameters of the regulators depicted in Fig. 4 are listed in Table II.

The control algorithms for the stator and rotor windings have been implemented with two independent five-phase inverters based on Infineon F12-25R12KT4G IGBT

modules, which are controlled by Texas Instruments floating-point DSPs.

The results reported in this section have been obtained by imposing  $E_{SDC}$  equal to 300 V through power supply TDK Lambda GEN600-5.5.

The reference value of the magnetizing current  $i_{s1d,ref}$  has been kept constant at 2.6 A, while the current  $i_{s1q,ref}$  requested by the speed controller (a) has been limited to  $\pm 4.6$  A. Consequently, the drive can produce any torque  $T_1$  between  $\pm 30$  Nm. The braking torque  $T_B$  is proportional to the angular speed of the motor and is equal to about 30 Nm at 70 rpm. The braking action is performed by a dc machine used as a generator.

During the tests, the current  $\bar{i}_{s3}$  has been set with a magnitude of 2.7 A and an angular speed  $\Delta\omega_3$  of 628.3 rad/s (100 Hz). The set-points of the currents and the angular speed  $\Delta\omega_3$  have been selected in order to deliver a power  $P_R$  of 200 W generating a small torque disturbance  $T_3$ , which is about 10% of  $T_1$ . This choice allows to treat the torque  $T_3$  as a minor disturbance that can be easily compensated by the speed control loop of the system.

The vector space decomposition of the stator currents when the speed of the rotor is 70 rpm and the power  $P_R$  is 150 W is shown Fig. 6. The phase current  $i_{sa}$  is composed of two harmonics. The low-frequency component is related to the torque  $T_1$  as described in Section II.B, while the high-frequency component is related to the power transferred to

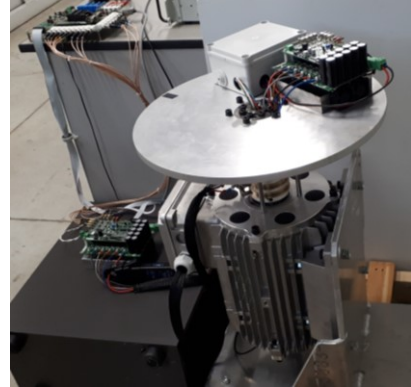


Fig. 5 - Pictures of the small-scale rotary assembly station setup.

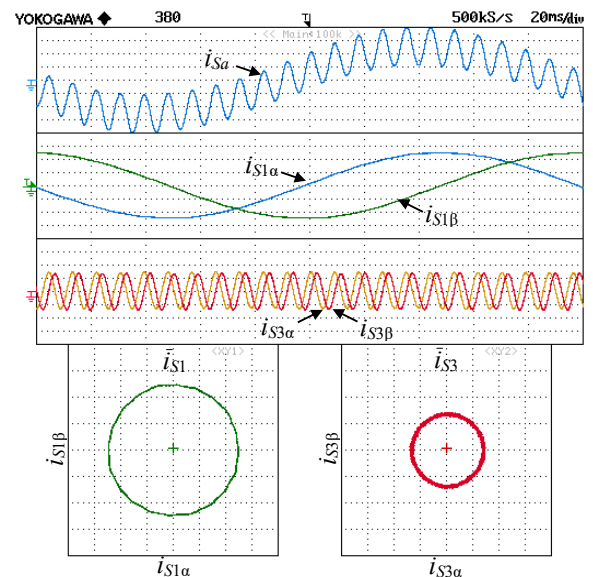


Fig. 6. Vector space decomposition of the stator currents at steady state. Waveforms of the stator phase current  $i_{sa}$  (2 A/div), current components  $i_{s1a}$  (2 A/div),  $i_{s1b}$  (2 A/div),  $i_{s3a}$  (2 A/div), and  $i_{s3b}$  (2 A/div).

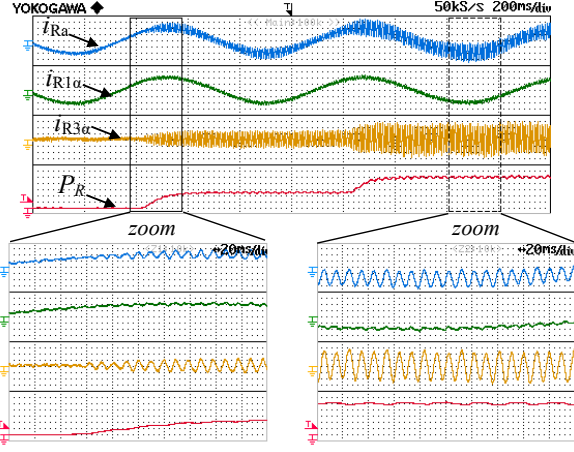


Fig. 7. Vector space decomposition of the rotor currents during a variation of the electric power absorbed by the rotor loads while the setpoint of the speed is 70 rpm and the braking torque  $T_R$  is 30 Nm. Waveforms of the rotor phase current  $I_{Ra}$  (1 A/div), the current component  $i_{R1a}$  (1 A/div), the current component  $i_{R3a}$  (0.5 A/div), and the power  $P_R$  (30 W/div).

the rotor loads as described in Section II.C. The loci of vectors  $\vec{i}_{S1}^S$  and  $\vec{i}_{S3}^S$  are circular trajectories traveled at different angular speeds.

Fig. 7 shows the vector space decomposition of the rotor currents when the mechanical speed is 70 rpm and the power  $P_R$  increases from 0 W to 150 W. With a good approximation, the current component  $i_{R1a}$ , which is related to the torque  $T_1$ , is a sinusoidal waveform with almost constant magnitude and frequency. Therefore, both the speed of the rotor and the torque contribution  $T_1$  are nearly constant and independent of  $P_R$ . Conversely, the magnitude of  $i_{R3a}$  rises if  $P_R$  increases, but the period of the waveform is constant and equal to 10 ms (100 Hz). According to the analysis presented in Section II, the torque disturbance  $T_3$  is generated when  $P_R$  is different from zero. During the tests, the torque  $T_3$  is theoretically equal to 2.9 Nm when  $P_R$  is 200 W. Therefore, a minimal variation of  $T_1$  is required to compensate  $T_3$  and control the speed of the machine.

Fig. 8 depicts the loci covered by current  $\vec{i}_{R3}$  in the plane  $i_{R3d} - i_{R3q}$  when  $P_R$  changes from 0 W to 200 W for several values of  $E_{RDC}$ . The curves on the left-end side of the picture have almost the same magnitude of the current component  $i_{R3d}$ , corresponding to a rotor power of 200 W. It is worth observing that the trajectory of  $\vec{i}_{R3}$  lies entirely on the d-axis only if  $E_{RDC}$  is equal to 270 V. In this case, the Joule loss of the rotor winding is minimized in the power range 0 W – 200 W. In the other cases, the maximum power that can be

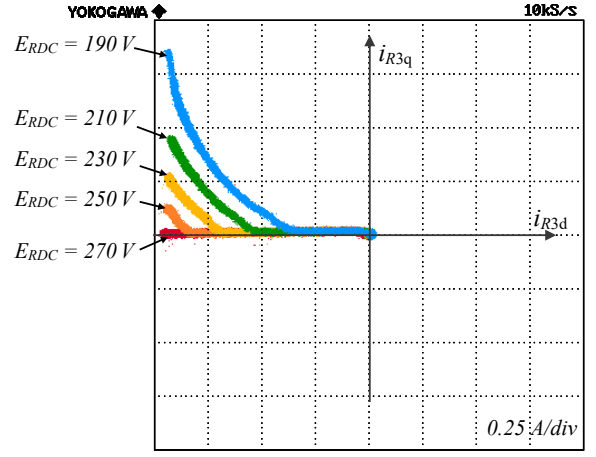


Fig. 8. Trajectories followed by current  $\vec{i}_{R3}$  in the plane  $i_{R3d} - i_{R3q}$  when the rotor power  $P_R$  changes from 0 W to 200 W for several values of voltage  $E_{RDC}$ .

obtained under the constraint  $i_{R3q} = 0$  decreases as the available voltage  $E_{RDC}$  reduces. Finally, higher levels of  $P_R$  can be obtained by injecting a positive current  $i_{R3q}$  in order to follow the trajectory that lies on the circumference described by the voltage limit in (41). Fig. 8 clearly shows that the proposed control scheme can operate the drive at the minimum rotor Joule losses and satisfying the current and voltage constraints (38) - (39). The proposed control strategy allows one to increase the power  $P_R$  by about 200 % respect to the control scheme of [6], using the same current magnitude  $I_{S3}$  and the same angular speed  $\Delta\omega_3$ . The detailed comparison between the proposed control scheme and the one presented in [6] is discussed in Appendix.

The behavior of the drive system during a working cycle for rotary assembly station has been emulated by setting a speed profile and an active power profile. Fig. 9 shows the estimated torque  $T_1$ , the mechanical speed  $\omega_m$ , the dc-link voltage of the rotor inverter  $E_{RDC}$  and the power extracted from the rotor winding  $P_R$ .

The experimental results proof that the proposed control system can independently control the speed of the rotating disk and the power transferred to the auxiliary actuators, as requested in industrial rotary assembly platforms.

## V. CONCLUSION

The paper investigates the use of a gearless five-phase doubly-fed induction machine in automation applications based on rotary tables. The aim of the drive is the independent control of the motion of the platform and the power transferred to the actuators and sensors located on the rotating disk. The integrated drive avoids using sliding contacts and ensure better continuity of service in automated production chains. The control scheme proposed in this paper maximizes the power transferred to the rotating loads in compliance with the thermal constraint of the rotor currents and the voltage constraint of the rotor inverter.

Furthermore, the operating limits of the drive are derived and shown in a graphical form for easier understanding. The control scheme is divided into two independent parts, one implemented on the stator inverter and one on the rotor inverter. Therefore, synchronization and information exchange between the two control systems are not necessary, leading to high system robustness. Experimental tests confirm the capability of the drive to control the rotor speed and the power supplied to the rotor loads independently.

TABLE I - PARAMETERS OF THE FIVE-PHASE MACHINE

$R_S = 1.7 \, \Omega$ , $R_R = 4.8 \, \Omega$	$T_{l, rated} = 50 \, \text{Nm}$
$L_{S1} = 411 \, \text{mH}$ , $L_{S3} = 68 \, \text{mH}$	$\omega_{m, rated} = 5.2 \, \text{rad/s}$ (50 rpm)
$L_{R1} = 939 \, \text{mH}$ , $L_{R3} = 158 \, \text{mH}$	$p = 3$
$M_1 = 555 \, \text{mH}$ , $M_3 = 53 \, \text{mH}$	Rotor turn-number $N_R = 89$
$I_{S, rated} = 4.8 \, \text{A}_{RMS}$ , $i_{R, rated} = 2.1 \, \text{A}_{RMS}$	Stator turn-number $N_S = 58$
$I_{S1d, rated} = 3.5 \, \text{A}$	

TABLE II - PARAMETERS OF THE REGULATORS

Speed regulator (a)	$k_p = 0.6 \, \text{A} \cdot \text{s/rad}$ , $k_i = 6.3 \, \text{A}$
Current regulators (b) and (c)	$k_p = 29 \, \Omega$ , $k_i = 600 \, \Omega/\text{s}$
Current regulators (d) and (e)	$k_p = 78 \, \Omega$ , $k_i = 2000 \, \Omega/\text{s}$
Current regulators (m) and (n)	$k_p = 66 \, \Omega$ , $k_i = 2000 \, \Omega/\text{s}$
$E_{RDC}$ regulator (h)	$k_p = 0.1 \, \Omega^{-1}$ , $k_i = 0.5 \, \Omega^{-1} \cdot \text{s}^{-1}$
Rotor voltage (i)	$k_p = 0.01 \, \Omega^{-1}$ , $k_i = 10 \, \Omega^{-1} \cdot \text{s}^{-1}$
Time constant $\tau_f$ used in (50) for the estimation of the flux $\vec{\varphi}_{R3}^R$	$\tau_f = 0.0318 \, \text{s}$ (5 Hz)

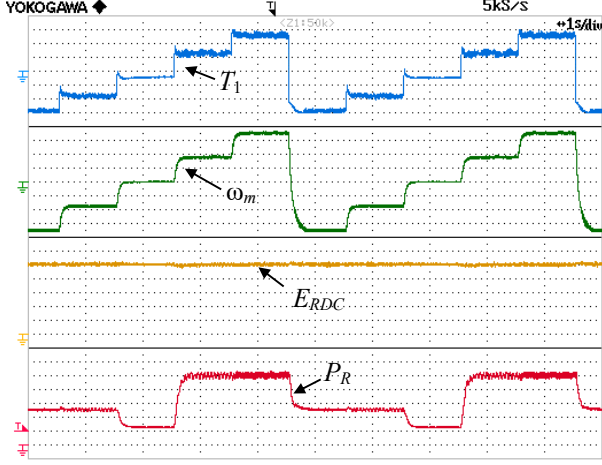


Fig. 9. Emulation of a generic working cycle for rotary assembly stations. Waveforms of the estimated torque  $T_1$  (4 Nm/div), mechanical speed  $\omega_m$  (10 rpm/div), rotor voltage  $E_{RDC}$  (20 V/div), and power  $P_R$  (20 W/div).

Lastly, the proposed control scheme adjusts the reactive power provided by the rotor inverter to minimize the Joule loss of the rotor winding.

#### APPENDIX

In the following, the difference in terms of maximum power transferred to the rotor loads between the method proposed in this paper and the one presented in [6] is discussed.

In [6], power  $P_R$  is extracted from the rotor winding using a direct power control scheme. The rotor inverter measures the current  $\bar{i}_{R3}$  and imposes a voltage  $\bar{v}_{R3,ref}$  in phase opposition, such as to extract the required power  $P_{R,ref}$ . This control scheme is very simple, and it does not require the injection of reactive power into the rotor winding. However, the dynamics of the rotor current is not controlled, and the current  $\bar{i}_{R3}$  is different from zero even when the power required to the load is zero, generating heat in the rotor winding.

Fig. 10 shows the trajectory followed by the current  $\bar{i}_{R3}$  when the control scheme in [6] is implemented. The output power  $P_R$  is zero in point 1, while in point 2 the power is maximum and it is equal to  $P_{R,max[6]}$ . The maximum power  $P_{R,max[6]}$  can be calculated by geometric relationships in the tangent conditions between the active and reactive power circles depicted in figure as follows:

$$x_{P_R}^2 + y_{Q_R}^2 = (r_{Q_R} + r_{P_R})^2. \quad (A1)$$

By considering (30), (34), (A1) and imposing  $Q_R = 0$ , it can be verified that  $P_{R,max[6]}$  is equal to

$$P_{R,max[6]} = \frac{5}{4} v_{exc}^2 \frac{\sqrt{R_R^2 + \Delta\omega^2 L_{R3}^2} - R_R}{\Delta\omega^2 L_{R3}^2}. \quad (A2)$$

Conversely, the control scheme proposed in this paper injects reactive power in the rotor circuit in order to minimize the Joule loss. This choice results in the condition  $i_{R3q} = 0$ . If the voltage constraint (39) is satisfied, the maximum power transferred to rotor loads of the proposed method is:

$$P_{R,max} = -\frac{5}{2} (R_R I_{R3,max}^2 + v_{exc} I_{R3,max}). \quad (A3)$$

To compare the power limit of the two control schemes, the same values of  $\Delta\omega$ , stator current magnitude  $I_{S3}$  and rotor

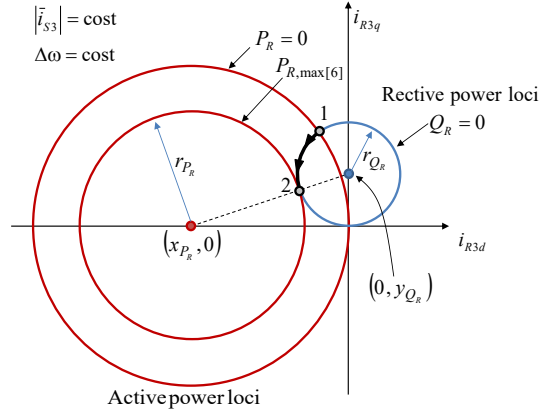


Fig. 10. Trajectory followed by current  $\bar{i}_{R3}$  when the control scheme in [6] is implemented.

current magnitude  $I_{R3}$  should be considered. As can be seen in Fig. 10, in [6] the maximum current occurs when  $P_R$  is zero and can be calculated, with a good approximation, as:

$$I_{R3,max[6]} \cong 2r_{Q_R} = \frac{v_{exc}}{\Delta\omega L_{R3}}. \quad (A4)$$

The maximum power achievable by the proposed control scheme, when the same rotor current is considered, can be obtained by introducing (A4) in (A3) as:

$$P_{R,max} = \frac{5}{2} v_{exc}^2 \frac{\Delta\omega L_{R3} - R_R}{\Delta\omega^2 L_{R3}^2}. \quad (A5)$$

The ratio between power (A5) and (A2) is then equal to:

$$\frac{P_{R,max}}{P_{R,max[6]}} = \frac{2(\Delta\omega L_{R3} - R_R)}{\sqrt{R_R^2 + \Delta\omega^2 L_{R3}^2} - R_R}. \quad (A6)$$

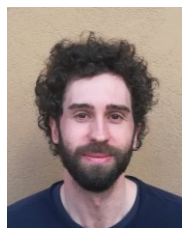
Equation (A6) shows that if  $\Delta\omega$  increases, the ratio between the powers tends to 2 regardless of the machine parameters. Under the conditions reported in the laboratory tests, this ratio is equal to 1.98. Therefore, the proposed method increases the power transferred to the rotor up to 200% with respect to [6], demonstrating a significant improvement.

#### REFERENCES

- [1] R. D. Hall and R. P. Roberge, "Carbon brush performance on slip rings," in *Proc. Pulp & Paper Ind. Tech. Conf.*, DOI 10.1109/PAPCON.2010.5556522, pp. 1-6, 2010.
- [2] R. Trevisan and A. Costanzo, "A 1-kW contactless energy transfer system based on a rotary transformer for sealing rollers," *IEEE Trans. Ind. Electron.*, vol. 61, DOI 10.1109/TIE.2014.2311395, no. 11, pp. 6337-6345, Nov. 2014.
- [3] J. Dai, S. Hagen, D. C. Ludois, and I. P. Brown, "Synchronous Generator Brushless Field Excitation and Voltage Regulation via Capacitive Coupling Through Journal Bearings," *IEEE Trans. Ind. Appl.*, vol. 53, DOI 10.1109/TIA.2017.2681621, no. 4, pp. 3317-3326, July-Aug. 2017.
- [4] J. Dai and D. C. Ludois, "A Survey of Wireless Power Transfer and a Critical Comparison of Inductive and Capacitive Coupling for Small Gap Applications," *IEEE Trans. Power Electron.*, vol. 30, DOI 10.1109/TPEL.2015.2415253, no. 11, pp. 6017-6029, Nov. 2015.
- [5] M. Mengoni, G. Rizzoli, L. Zarri, A. Tani, A. Amerise, and G. Serra, "Control of a Three-Phase Wound-Rotor Induction Motor Drive for Automation Applications," in *Proc. Int. Elec. Machines & Drives Conf. (IEMDC)*, DOI 10.1109/IEMDC.2019.8785281, pp. 1267-1272, 2019.
- [6] G. Rizzoli, M. Mengoni, A. Tani, G. Serra, L. Zarri, and D. Casadei, "Wireless Power Transfer Using a Five-Phase Wound-Rotor Induction Machine for Speed-Controlled Rotary Platforms," *IEEE Trans. Ind. Electron.*, Vol. 67, DOI 10.1109/TIE.2019.2935988, No. 8, pp. 6237 - 6247, Aug. 2020.
- [7] G. Rizzoli, M. Mengoni, G. Sala, L. Zarri, and A. Tani, "Control of the Torque and Rotor Power in a Five-Phase Wound-Rotor Induction Motor Drive for Rotary Assembly Platforms," in *Proc. Int. Conf. on Elec. Machines (ICEM)*, DOI 10.1109/ICEM49940.2020.9270773, pp. 2090-2096, 2020.



- [8] E. Levi, "Advances in converter control and innovative exploitation of additional degrees of freedom for multiphase machines," *IEEE Trans. Ind. Electron.*, vol. 63, DOI 10.1109/TIE.2015.2434999, No. 1, pp. 433 - 448, Jan. 2016.
- [9] M. J. Duran and F. Barrero, "Recent Advances in the Design, Modeling, and Control of Multiphase Machines—Part II," *IEEE Trans. on Ind. Electron.*, vol. 63, DOI 10.1109/TIE.2015.2448211, no. 1, pp. 459-468, Jan. 2016.
- [10] N. Bianchi, S. Bolognani, and M. Dai Pre, "Strategies for the Fault-Tolerant Current Control of a Five-Phase Permanent-Magnet Motor," *IEEE Trans. Ind. Appl.*, vol. 43, DOI 10.1109/TIA.2007.900445, no. 4, pp. 960-970, July-Aug. 2007.
- [11] M. J. Duran, I. Gonzalez-Prieto, N. Rios-Garcia, and F. Barrero, "A Simple, Fast, and Robust Open-Phase Fault Detection Technique for Six-Phase Induction Motor Drives," *IEEE Trans. on Power Electron.*, vol. 33, DOI: 10.1109/TPEL.2017.2670924, no. 1, pp. 547-557, Jan. 2018.
- [12] A. Shawier, A. S. Abdel-Khalik, R. A. Hamdy, K. H. Ahmed, and S. Ahmed, "Postfault Operation of Five-Phase Induction Machine with Minimum Total Losses Under Single Open-Phase Fault," *IEEE Access*, vol. 8, DOI: 10.1109/ACCESS.2020.3036904, pp. 208696-208706, 2020.
- [13] H. Liu, D. Wang, X. Yi, and F. Meng, "Torque Ripple Suppression Under Open-Phase Fault Conditions in a Five-Phase Induction Motor With Harmonic Injection," *IEEE J. Emerg. Sel. Topics Power Electron.*, vol. 9, DOI: 10.1109/JESTPE.2019.2952374, no. 1, pp. 274-288, Feb. 2021.
- [14] L. Parsa, N. Kim, and H. A. Toliyat, "Field Weakening Operation of High Torque Density Five-Phase Permanent Magnet Motor Drives," in *Proc. Int. Conf. on Elec. Machines and Drives*, DOI 10.1109/IEMDC.2005.195920, pp. 1507-1512, 2005.
- [15] S. Khadar, H. Abu-Rub, and A. Kouzou, "Sensorless Field-Oriented Control for Open-End Winding Five-Phase Induction Motor with Parameters Estimation," *IEEE Open J. of the Ind. Electron. Soc.*, vol. 2, DOI: 10.1109/OJIES.2021.3072232, pp. 266-279, 2021.
- [16] A. G. Yepes et al., "Selection Criteria of Multiphase Induction Machines for Speed-Sensorless Drives Based on Rotor Slot Harmonics," *IEEE Trans. Ind. Electron.*, vol. 63, DOI: 10.1109/TIE.2016.2548979 no. 8, pp. 4663-4673, Aug. 2016.
- [17] M. Trabelsi, N. K. Nguyen, and E. Semail, "Real-Time Switches Fault Diagnosis Based on Typical Operating Characteristics of Five-Phase Permanent-Magnetic Synchronous Machines," *IEEE Trans. Ind. Electron.*, vol. 63, DOI 10.1109/TIE.2016.2554540, no. 8, pp. 4683-4694, Aug. 2016.
- [18] I. Subotic, O. Dordevic, J. B. Gomm, and E. Levi, "Active and Reactive Power Sharing Between Three-Phase Winding Sets of a Multiphase Induction Machine," *IEEE Trans. Energy Convers.*, vol. 34, DOI: 10.1109/TEC.2019.2898545, no. 3, pp. 1401-1410, Sept. 2019.
- [19] D. E. Levi, D. Dujic, M. Jones, and G. Grandi, "Analytical Determination of DC-Bus Utilization Limits in Multiphase VSI Supplied AC Drives," *IEEE Trans. on Energy Conversion*, vol. 23, DOI 10.1109/TEC.2008.921557, no. 2, pp. 433-443, June 2008.
- [20] L. Harnefors and M. Hinkkanen, "Stabilization Methods for Sensorless Induction Motor Drives - A Survey," *IEEE J. Emerg. Sel. Topics Power Electron.*, vol. 2, DOI 10.1109/JESTPE.2013.2294377, no. 2, pp. 132-142, June 2014.



**Gabriele Rizzoli** received the M.Sc. and Ph.D. degree in Electrical Engineering respectively in 2012 and 2016, from the University of Bologna, Bologna, Italy. He is currently a Junior Assistant Professor at the Department of Electrical, Electronic and Information Engineering "G. Marconi" of the University of Bologna.

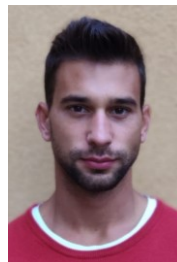
His research interests include the design of electrical machines, the development and control of high-efficient power converters for automotive and renewable energy applications.



**Michele Mengoni** (M'13) received the M.S. (with honors) and Ph.D. degrees in electrical engineering from the University of Bologna, Bologna, Italy, in 2006 and 2010, respectively. He is currently an Associate Professor with the Department of Electrical, Electronic and Information Engineering "G. Marconi", University of Bologna. His research interests include design, analysis, and control of three phase electric machines, multiphase drives, and ac/ac matrix converters.



**Giacomo Sala** (M'18) received the B.Sc. degree in power engineering, the M.Sc. degree (hons.) in electrical engineering, and the Ph.D. degree in electrical machines and drives from the University of Bologna, Bologna, Italy, in 2012, 2014, and 2018, respectively. Until 2019, he was as a Researcher with the Power Electronics, Machines and Control Group, Department of Electrical and Electronic Engineering, The University of Nottingham, Nottingham, U.K. Since 2019, he has been a Researcher with the Department of Electrical, Electronic, and Information Engineering "Guglielmo Marconi", University of Bologna, where he has been a Junior Assistant Professor, since 2020. His research interests include design, modeling, and control of multiphase electrical machines, fault-tolerant control, and fault diagnosis of electric drives.



**Luca Vancini** received the M.Sc. degree in Electrical Engineering in 2018 from the University of Bologna, Bologna, Italy. Currently he is pursuing a PhD in electrical engineering with the Department of Electrical, Electronic and Information Engineering "G. Marconi", University of Bologna. His research interests include power electronics, control of multiphase converters and diagnostic techniques for multiphase machines.



**Luca Zarri** (M'05-SM'12) received the M. Sc. degree (hons.) and the Ph.D. degree in Electrical Engineering from the University of Bologna, Bologna, Italy, respectively in 1998 and 2007. He worked as a freelance software programmer from 1989 to 1992 and as a plant designer with an engineering company from 1998 to 2002. In 2003 he became a laboratory engineer with the Department of Electrical, Electronic and Information Engineering "G. Marconi", University of Bologna, where he is currently a Full Professor of Power Electronics and Electric Drives. He is author or co-author of more than 170 scientific papers. His research activity concerns the control of power converters and electric drives. Prof. Zarri is a senior member of the IEEE Industry Applications, IEEE Power Electronics, and IEEE Industrial Electronics Societies. At present, he serves as the Paper Review Chair for the IEEE IAS Industrial Drives Committee.



**Angelo Tani** received the M. Sc. degree (hons.) in Electrical Engineering from the University of Bologna, Bologna, Italy, in 1988. Currently, he is a Full Professor of power electronics, electrical machines and drives with the Department of Electrical, Electronic and Information Engineering "G. Marconi", University of Bologna. He has authored more than 180 papers published in technical journals and conference proceedings. His current activities include multiphase and three phase electric drives, diagnostic techniques for electric machines, and active filters.



**Radu Bojoi** (F'19) received the M.Sc. degree from Technical University of Iasi, Iasi, Romania, in 1993, and the Ph.D. degree from Politecnico di Torino, Torino, Italy, in 2002, all in electrical engineering. He is currently a Full Professor of Power Electronics and Electrical Drives with the Energy Department G. Ferraris and Chairman of the Power Electronics Innovation Center, Politecnico di Torino, Italy. He has authored or coauthored more than 150 papers covering electrical drives and power electronics for industrial applications, transportation electrification, power quality, and home appliances. He was involved in many research projects with industry for direct technology transfer aiming at obtaining new products. Prof. Bojoi is the corecipient of five prize paper awards, the last one in 2015 as IEEE-IAS Prize Paper Award. He is a Co-Editor-In-Chief of the IEEE TRANSACTIONS ON INDUSTRIAL ELECTRONICS and Chair of the Electrical Machines Technical Committee of the Industrial Electronics Society.